ARTICLE

Structure–Property Relationships in Porous 3D Nanostructures: Epoxy-Cross-Linked Silica Aerogels Produced Using Ethanol as the Solvent

Mary Ann B. Meador,*,† Amanda S. Weber,‡ Alia Hindi,‡ Melanie Naumenko,‡ Linda McCorkle,§ Derek Quade,† Stephanie L. Vivod,† George L. Gould,⊥ Shannon White,⊥ and Kiranmayi Deshpande⊥

NASA Glenn Research Center, 21000 Brookpark Road, Cleveland, Ohio 44135, and Aspen Aerogels, Northborough, Massachusetts 01532

ABSTRACT Cross-linking silica aerogels with organic groups has been shown to improve the strength over un-cross-linked aerogels by as much as 2 orders of magnitude. Previous cross-linking chemistry has been developed using solvents specifically chosen to dissolve the monomers and accommodate the reaction temperature. Because the process of making the aerogels requires so much solvent, it is of interest to consider less toxic solvents such as ethanol to increase safety and enhance scale up. To this end, two different epoxy precursors with suitable solubility in ethanol were evaluated as cross-linkers for silica gels prepared from (3-aminopropyl)triethoxysilane and tetraethylorthosilicate. In addition, 1,6-bis(trimethoxysilyl)hexane (BTMSH) was used as an additive in the underlying silica structure to add flexibility to the aerogels. It was found that the ethanol-derived aerogels exhibited more shrinkage than those prepared from other solvents but that including BTMSH in the aerogels significantly reduced this shrinkage. Inclusion of BTMSH also imparted the ability of the aerogel monoliths to recover elastically when compressed up to 50% strain. In addition, optimized cross-linked aerogels prepared in this study have mechanical properties comparable to those using other more undesirable solvents and cross-linkers.

KEYWORDS: aerogel • polymer cross-linking • nanoporous materials • hybrid materials • sol–gel

INTRODUCTION

Silica aerogels with their low density, large internal surface areas, and very small pore size are potential candidates for various thermal, optical, and acoustic applications (1). However, the use of aerogel monoliths has been restricted because of their poor mechanical properties. It has been demonstrated that by cross-linking the silica skeleton with diisocyanates through the silanol surface the strength is improved by as much as 2 orders of magnitude while only doubling the density over those of native, or non-cross-linked, aerogels (2). In addition, the mesoporosity of the cross-linked aerogels is maintained. Hence, their superior insulating properties are preserved. Incorporating a functional group such as amine or vinyl on a silica precursor into a silica-based aerogel improves the cross-linking with isocyanates (3, 4) while expanding the types of organic groups that can be used as cross-linkers to include epoxies (5) and styrene (6). Other approaches to strengthening the silica aerogel structure by incorporation of a polymer include dispersing functionalized polymer nanoparticles in a silica network (7) and copolymerization of silica precursors with poly(methyl methacrylate) and poly(dimethylacrylamide) (8) or poly(vinylpyrrolidone) (9).

Improvements to the mechanical properties of aerogels realized by reinforcing the silica structure with polymer enable the design of customized, lightweight, multifunctional structures (including insulation, sound dampening, and structural support) for aircraft, rotorcraft, space vehicles, extravehicular activity suits, and habitats that may be enabling for future NASA missions. In addition, if manufacturing costs of polymer cross-linked aerogels can be decreased, down-to-earth applications, including insulation for refrigeration, housing construction, and industrial pipelines, can be realized.

Previously, we have used tetramethylorthosilicate (TMOS) as the main silica precursor for making the aerogels, and solvent choice has been largely dictated by the solubility of the monomers and the cure temperature of cross-linking chemistry. In order to scale up manufacturing processes for cross-linking aerogels, it is desirable to adopt the use of less toxic tetraethylorthosilicate (TEOS) as a silica precursor and ethanol, a more industrially friendly solvent. Two epoxy monomers, resorcinol diglycidyl ether (RGE) and bisphenol A propoxylate diglycidyl ether (BPGE), shown below, are identified to have suitable solubility in ethanol.

* To whom correspondence should be addressed. E-mail: maryann.meador@nasa.gov.
Received for review January 7, 2009 and accepted March 2, 2009
† NASA Glenn Research Center.
‡ NASA Undergraduate Student Intern.
§ Employed by the Ohio Aerospace Institute.
⊥ Aspen Aerogels.
DOI: 10.1021/am900014z

Published on Web 04/02/2009

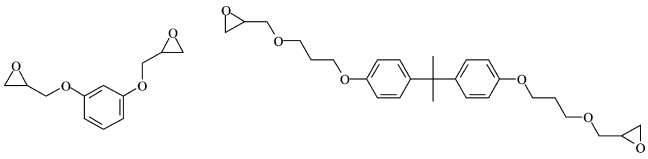

RGE BPGE

In this paper, we discuss the use of these epoxies to cross-link TEOS-derived gels using ethanol as the solvent. (3-Aminopropyl)triethoxysilane (APTES) is used as a coreactant with TEOS to create amine sites to react with epoxy on the surface of the silica gels, as shown in Scheme 1. In addition, 1,6-bis(trimethoxysilyl)hexane (BTMSH) is investigated as an extra modifier of the underlying silica gel. BTMSH and other bridged monomers have been used as precursors for both aerogel and xerogel forms of silsesquioxanes (10). Incorporation of this type of flexible bridging group was found to lead to more compliant materials. The six-carbon-bridged BTMSH has been shown to gel in less than 1 h, while smaller bridges can cause the formation of cyclic structures, which drastically slow or prevent gelation altogether (11). Alkyl bridges longer than six carbons, in general, produce larger pore sizes and wider pore-size distributions (12), perhaps leading to reduced surface areas and increased thermal conductivity. We have recently demonstrated that using BTMSH as a modifier in styrene-cross-linked aerogels resulted in nearly complete recovery after compression to 25% strain for certain formulations while maintaining a Young's modulus of ~2 MPa (13). Herein, we replace up to 40 mol % of the Si atoms in the underlying gel with BTMSH-derived Si. Scheme 2 shows a comparison of the molecular structure for an APTES-modified silica backbone without incorporation of BTMSH-derived Si and with 40 mol % BTMSH-derived Si. Note that the regions of pure SiO_2 are greatly reduced, leading to a more open skeletal nanostructure. The effects of this type of structure on the mechanical properties, surface area, and pore structure of the epoxy-cross-linked aerogels are examined. Statistical experimental design methodology is used to derive empirical models and enhance the understanding of the significant relationships between variables used to prepare the aerogels and the resulting properties.

EXPERIMENTAL SECTION

Materials. Tetramethylorthosilicate (TMOS), tetraethylorthosilicate (TEOS), 1,6-bis(trimethoxysilyl)hexane (BTMSH), and (3-aminopropyl)triethoxysilane (APTES) were purchased from Gelest, Inc. Resorcinol diglycidyl ether (RGE) and bisphenol A propoxylate diglycidyl ether (BPGE) were purchased from Aldrich Chemical Company. Ethanol (100%) was purchased from Pharmco Products, Inc. All reagents were used without further purification.

Instrumentation. Supercritical fluid extraction was carried out with an Applied Separations 1 L SPE-ED SFE-2. Solid ^{29}Si and ^{13}C NMR spectra of the aerogels were obtained on a Bruker Avance 300 spectrometer using a 4 mm solids probe with cross-polarization and magic angle spinning at 11 kHz. ^{13}C NMR spectra were externally referenced to the carbonyl of glycine, which appears at 176.1 ppm relative to tetramethylsilane. ^{29}Si NMR spectra were externally referenced to 3-(trimethoxysilyl)-propionic acid at 0 ppm. Samples for microscopy were coated with gold/palladium and viewed using a Hitachi S-4700-11 field-emission scanning electron microscope. Skeletal densities of the aerogels were obtained on a Micromeritics Accupyc 1340 helium pycnometer. Nitrogen sorption porosimetry was carried out on an ASAP 2000 surface area/pore-size distribution analyzer (Micromeritics Instrument Corp.). Samples were outgassed by heating at 60 °C under vacuum for 24 h prior to testing.

Scheme 1. Typical Reaction Scheme for Cross-Linking Silica Gels with Epoxy through Surface Amine Groups

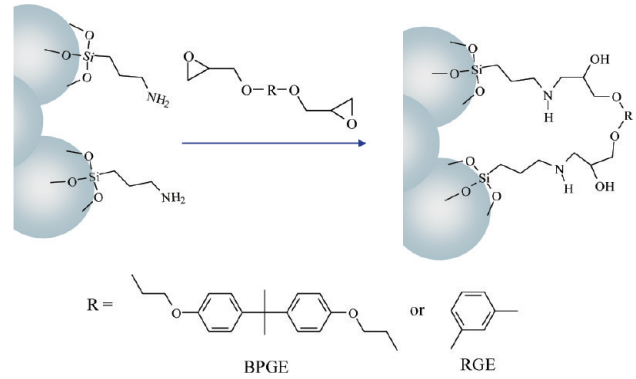

Aerogel Fabrication. Cross-linked aerogels were prepared starting with a sol–gel process similar to those previously described (3) except that ethanol is used as a solvent instead of acetonitrile. The concentration of the copolymerized silanes (TEOS or TMOS, APTES, and BTMSH) in the starting gels was varied as described in Tables 1–3, where the concentration of the total Si is expressed as mol/L of the total sol. It should be noted that the concentration is expressed in mol/L of Si instead of mol/L of silane to account for the fact that BTMSH contributes two Si to the total silica content while TMOS, TEOS, and APTES contribute only one. The fraction of the total Si contributed by APTES and BTMSH is given in the tables as mol % of the total Si, with TMOS or TEOS being the remaining fraction. The concentrations of the epoxy in the cross-linking baths to which the gels are exposed are given as w/w % of the total ethanol soak solution. A concentration of 15 w/w % epoxy in ethanol was used for all runs listed in Tables 1 and 3, while the concentration was varied between 15 and 25 w/w % as listed in Table 2. Two example preparations are given for TMOS- and TEOS-derived aerogels.

TMOS-Derived Aerogels. Amine-modified silica gels were produced as previously reported by combining two separate solutions, designated as A and B, in a sol–gel process. A typical procedure using run 1 in Table 1 in a 100 mL batch is given as an example. For solution A, 12.5 mL of TMOS (0.085 mol) and 3.5 mL of APTES (0.015 mol) were dissolved in 34 mL of ethanol. Solution B was prepared with 37.4 mL of ethanol and 12.6 mL of water (0.7 mol, based on a 7:1 mole ratio of water to total Si). Both solutions were cooled in a dry ice–acetone bath for about 5 min to slow gelation when combined. The use of amine-rich APTES eliminates the need for additional base catalysis. Five Norm-ject 20 mL polypropylene syringes, nominally 20 mm diameter, were prepared for use as molds by cutting off the needle end, extending the plunger nearly all the way out, and standing them in empty jars, with the plunger down for support. The contents of solution B were then poured into the container with solution A, which was capped immediately and shaken vigorously. The 100 mL total solution was poured into the molds, which were immediately covered with parafilm. The solutions were allowed to gel and age for a total of 24 h. The wet gels were extracted into clean ethanol at least 5 times the volume by inverting the syringes and depressing

Scheme 2. Underlying Silica Backbone Structure When Using (a) Approximately 20 mol % APTES-Derived Si and (b) Approximately 20 mol % APTES-Derived Si and 40 mol % BTMSH-Derived Si

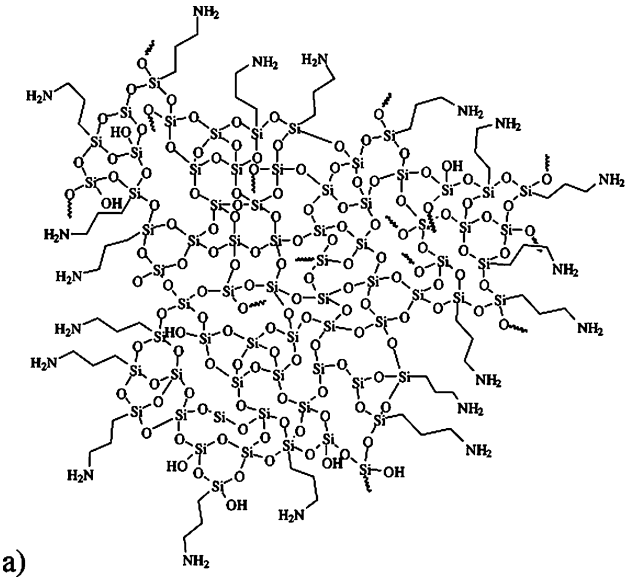

a)

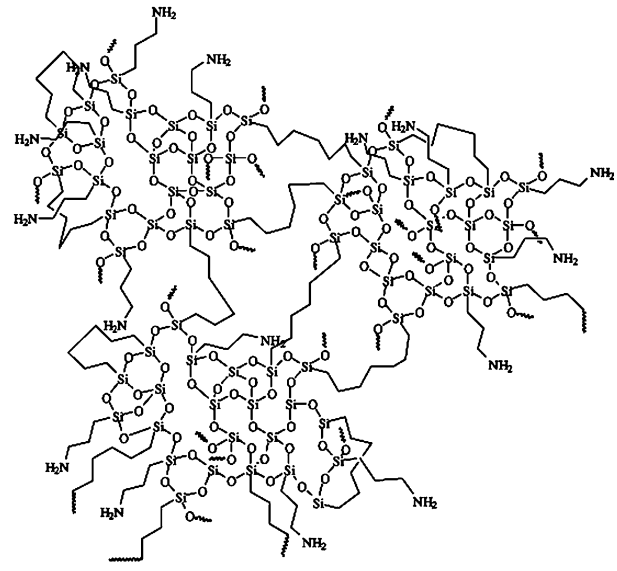

b)

Table 1. Summary of Data from an Initial Screening Study Comparing BPGE and RGE Cross-Linked Aerogels

run	total Si, mol/L	epoxy type	APTES Si, mol %	density, g/cm^3	porosity, %	shrinkage, %
1	1.00	BPGE	15	0.269	81.59	23.70
2	0.6	RGE	45	0.094	92.10	8.01
3	1.00	RGE	75	0.097	92.31	10.82
4	0.60	BPGE	75	0.107	91.19	25.79
5	0.20	BPGE	15	0.100	92.31	39.12
6	1.00	RGE	75	0.098	91.47	9.13
7	1.00	BPGE	45	0.349	74.06	26.94
8	0.20	RGE	15	0.057	95.58	32.37
9	0.20	RGE	15	0.056	96.22	30.22
10	1.00	RGE	15	0.205	87.30	18.12
11	1.00	BPGE	75	0.208	84.39	28.56
12	0.20	BPGE	45	0.058	95.71	27.05
13	0.6	BPGE	15	0.277	78.92	38.19
14	0.4	BPGE	15	0.223	84.10	41.12
16	0.4	RGE	75	0.036	97.40	17.77
17	0.4	RGE	15	0.141	91.08	33.41
18	0.4	RGE	15	0.185	88.18	38.58
19	0.4	BPGE	45	0.166	88.03	30.30

the plunger. The gels rested in ethanol for 24 h, and then ethanol was exchanged an additional three times at 24 h intervals to remove excess water and the condensation byproduct (methanol). To cross-link with epoxy, the ethanol in each of the five wet-gel containers was replaced with a 15 % w/w solution of BPGE in ethanol (60 g of BPGE in 340 g or 431 mL of ethanol) for 24 h with intermittent agitation. Afterward, the monomer solution was decanted and replaced with fresh ethanol, and the monoliths were allowed to react for 24 h in a 70 °C oven. The oven-cured gels were then cooled to room temperature, and ethanol was replaced four more times in 24 h intervals as before to remove any unreacted monomer or oligomers from the mesopores of the wet gels. These gels were then placed in a 1 L supercritical fluid-extraction chamber where ethanol was exchanged with liquid CO_2 at ~100 bar and 25 °C in five 2 h cycles. Heating the chamber to 45 °C causes the pressure to increase to ~215 bar, converting CO_2 to a supercritical state. Slow, controlled venting of the chamber gives the resulting epoxy cross-linked aerogel monoliths with an average bulk density of 0.269 g/cm^3.

TEOS-Derived Aerogels. TEOS-derived gels were made using a modified two-step process involving acid hydrolysis of TEOS, followed by base-catalyzed condensation with APTES (and BTMSH if used). To illustrate, a typical procedure is outlined using run 4 of Table 2 in a 100 mL batch as an example. To a solution of 16 mL of TEOS (0.072 mol) in 19.8 mL of ethanol was added a solution of 8.7 mL of water (0.48 mol, based on a 3:1 ratio of water to total Si) and 0.018 mL of nitric acid in 19.8 mL of ethanol with stirring. The combined solution A was stirred for 1 h. In the meantime, solution B was prepared, consisting 5.7 mL of APTES (0.024 mol) and 10.3 mL of BTMSH (0.032 mol but contributing 0.064 mol of Si) in 19.8 mL of ethanol A. Both solutions were then cooled in dry ice−acetone for 5 min, before pouring solution B into solution A and shaking vigorously. The combined 100 mL solution was then poured into molds as described above. The gels that formed in 1−50 min were aged for 24 h before extraction into clean ethanol. The gels rested in ethanol for 24 h, and then ethanol was exchanged one more time after a 24 h interval to remove excess water. To cross-link with epoxy, the ethanol in each of the five wet-gel containers was replaced with a 15 % w/w solution of BPGE in ethanol (60 g of BPGE in 340 g or 431 mL of ethanol) for 24 h with intermittent agitation. Afterward, the monomer solution was decanted and replaced with fresh ethanol, and the monoliths were allowed to react for 24 h in a 70 °C oven. After four additional solvent exchanges, the gels were dried by supercritical CO_2 fluid extraction followed by vacuum drying as described above to give monoliths with an average density of 0.233 g/cm^3.

Compression Tests. A cylindrical specimen from each run was sectioned in half with a scroll saw or razor blade (softer samples). The top and bottom of each specimen were sanded and checked using an L-square to make certain that these surfaces were smooth and parallel. The samples were tested between a pair of compression platens on an Instron model 4505 load frame using the Series IX data acquisition software. The platen surfaces were coated with a graphite lubricant to reduce the surface friction and barreling of the specimen. The specimens were tested in accordance with ASTM D695 with the exception of the sample size. Although the ASTM standard calls

Table 2. Summary of Data for Epoxy-Cross-Linked Aerogels from an Optimization Study

run	total Si, mol/L	APTES Si, mol %	BTMSH Si, mol %	BPGE concn, w/w %	density, g/cm^3	porosity, %	shrinkage, %	modulus, MPa	recovered strain, %	surface area, m^2/g	ave pore diameter, nm
1	1.6	15	0	15	0.373	72.91	15.26	58.34	0.20	361.69	15
2	1	30	0	15	0.265	81.99	15.03	21.36	0.07	286.13	25
3	1.6	45	0	15	0.338	75.99	11.41	50.61	*a*	212.42	24
4	1.6	15	40	15	0.233	83.45	6.72	10.46	0.24	375.02	22
5	1.6	15	40	15	0.233	83.44	4.89	14.04	0.23	304.92	26
6	1.6	30	20	15	0.309	77.90	7.29	38.82	0.13	253.97	24
7	1.6	45	0	15	0.382	71.96	11.19	97.81	0.14	212.64	22
8	1.6	45	40	15	0.375	70.75	12.86	30.22	0.09	104.00	27
9	1	45	20	15	0.188	85.92	7.43	6.41	0.12	170.4	27
10	1	30	20	15	0.188	86.12	8.23	9.56	0.12	237.2	21
11	1	30	20	15	0.189	86.45	8.28	11.37	0.20	217.08	26
12	1	15	20	15	0.176	87.73	11.83	4.22	0.21	324.83	25
13	1	30	40	15	0.186	85.54	7.25	5.78	0.24	172.92	30
14	0.8	15	0	15	0.230	85.66	22.14	12.51	0.17	301.53	26
15	0.8	15	0	25	0.244	85.27	22.88	13.26	0.14	289.77	27
16	0.8	15	40	20	0.127	91.39	11.37	1.40	0.15	323.36	25
17	0.8	45	0	20	0.177	86.82	8.50	5.57	0.10	209.52	35
18	0.8	45	40	15	0.160	88.31	13.78	2.42	0.14	107.58	28
19	0.8	45	40	25	0.180	86.59	12.34	3.83	0.16	102.58	36
20	1.2	15	0	20	0.291	81.26	18.87	21.76	0.17	315.01	15
21	1.6	15	40	25	0.239	82.55	6.36	6.54	0.13	314.79	28
22	1.6	45	0	25	0.318	78.50	6.02	35.22	0.18	198.24	24
23	1.6	45	40	25	0.394	69.72	10.79	49.10	0.11	99.12	30
24	1	30	20	15	0.192	86.72	8.46	7.92	0.11	244.65	25
25	1	30	20	15	0.193	86.57	8.27	4.40	0.17	*b*	*b*
26	1	30	20	15	0.196	87.05	8.10	7.00	0.16	*b*	*b*

[a] Sample broke before 25% strain. [b] Not measured.

Table 3. Preparation Conditions and Data for Monoliths Made with 0.4 mol/L Total Silane and Cross-Linked with 15 w/w % BPGE

run	APTES Si, mol %	BTMSH Si, mol %	density, g/cm^3	porosity, %	shrinkage, %	modulus, MPa	recovered strain, %
1	45.00	0.00	0.078	94.21	11.30	0.18	19.5
2	15.00	0.00	0.111	92.58	21.38	1.1	11.7
3	30.00	20.00	0.076	94.66	12.36	0.36	21.5
4	45.00	0.00	0.086	93.88	12.14	0.72	18.5
5	45.00	40.00	0.047	96.41	4.09	0.05	25
6	15.00	40.00	0.063	95.23	16.54	0.15	15.2

for a slenderness ratio of 11−16:1, typified by a cylinder of 12.7 mm in diameter by 50.8 mm in length, using this sample size would cause lower-density (more foamlike) specimens to buckle. In this study, the samples are nominally 16−18 mm in diameter and about 25−30 mm in length with a slenderness ratio of about 6−7:1.

Load−unload tests were also performed to determine the extent to which the samples recover after compression. In this case, samples were prepared identically to those for straight compression and the tests were carried out in the same manner except that the test was stopped at 25% strain. The sample was then recompressed to 25% strain, and then the load was removed. The specimens were allowed to recover for 30 min, at which time the sample length was measured. The amount of recovered strain listed in Table 2 is reported as the percent sample length recovered after the first compression. The amount of recovered strain measured after the second compression had greater random error, and hence it was not used in the statistical modeling.

Statistical Analysis. Experimental design and analysis was conducted using Design Expert Version 7.1, available from Stat-Ease, Inc., Minneapolis, MN. Multiple linear regression analysis was used to derive empirical models to describe the effect of each of the process variables studied on measured properties. A full quadratic model including all main effects, second-order effects, and all two-way interactions was entertained, and all variables were orthogonalized (transformed to −1 to +1 scale) before analysis. Terms deemed to not be significant in the model (<90% confidence) were eliminated one at a time using a backward stepwise regression technique.

RESULTS AND DISCUSSION

Comparison of RGE and BPGE Epoxy Cross-Linkers. An initial study was carried out to identify a preferred epoxy to be used between RGE and BPGE, with consideration of its solubility in ethanol and the effect on the characteristics of the final aerogel monoliths. This initial study also attempted to test the limits for the total Si concentration and the fraction of Si from APTES to reliably make intact aerogels. Thus, a range of total silane (TMOS

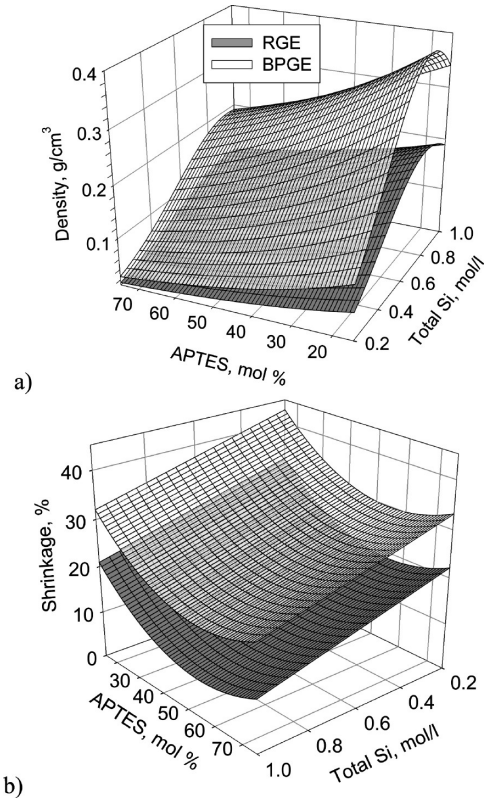

FIGURE 1. Graphs of empirical models of data from Table 1 for (a) density and (b) shrinkage during fabrication plotted vs mol % of Si derived from APTES and the total Si concentration for each of the two epoxies.

and APTES) from 0.2 to 1 mol/L based on the concentration in the total sol and the APTES fraction from 15 to 75 mol % was examined. The preparation conditions and measured properties from 19 aerogel formulations are compiled in Table 1. Graphs of the empirical models for density and shrinkage are shown in Figure 1.

The bulk density ranged from 0.035 up to 0.35 g/cm^3 across the whole screening study. In the empirical model for density (standard error = 0.015 g/cm^3; $R^2 = 0.98$), all main effect terms, as well as a second-order effect of the BTMSH fraction and synergistic/interactive terms for the total Si with the APTES fraction, APTES with the BTMSH fraction, and the epoxy type with the BTMSH fraction, were found to be significant. Graphs of the response surface model in Figure 1a show that a higher density is always achieved with BPGE as the epoxy. The molecular weight of BPGE compared to RGE may account for some of this increase. However, BPGE-cross-linked aerogels also tended to shrink more than RGE-cross-linked aerogels, as seen in the empirical model for shrinkage (Figure 1b), which also accounts for the higher density. The main difference between BPGE and RGE is the propoxylate groups in BPGE, lending perhaps a greater degree of flexibility to BPGE and also more affinity to the ethanol solvent. The increase in shrinkage may be due to collapse of the less rigid cross-link or greater retention of solvent after solvent exchange with CO_2 and before supercritical drying. The solvent in the gels is exchanged five times with liquid CO_2 before taking it to the supercritical point. Any ethanol remaining in the gels at this point would cause some collapse of the structure.

As expected, increasing the total Si in the monoliths also increases the density (more silica content) while increasing the APTES fraction slightly decreases the density. The latter is probably due to a decrease in shrinkage over the course of processing, as shown in the empirical graph in Figure 1b. In the model for shrinkage, it is shown that increasing the APTES fraction significantly decreases shrinkage. In the absence of such a trend for shrinkage, increasing APTES should increase the density by providing more amine sites for epoxy cross-linking. Thus, the decrease in shrinkage with an increasing amount of APTES is most likely due to the greater amount of polymer cross-linking reinforcing the aerogel skeleton.

Though BPGE-derived aerogels tend to shrink more than RGE-cross-linked aerogels, nevertheless, BPGE is chosen as the better epoxy cross-linker. BPGE is more soluble in ethanol, going readily into solution up to 25 w/w % concentration. RGE only sluggishly goes into solution with heating and stirring at even 20 w/w %, limiting the concentration of the cross-linking solution. Hence, BPGE was used through the rest of the study.

Comparison of TMOS and TEOS. To compare epoxy-cross-linked aerogels made from TMOS and APTES to those made from TEOS and APTES, a formulation of the BPGE-cross-linked aerogels was chosen that had a total Si concentration of 0.6 mol/L and 15 mol % APTES (run 13 from Table 1). Several batches of each of the formulations (TEOS- and TMOS-derived) were fabricated using the following procedures discussed in more detail in the Experimental Section. TMOS-derived aerogels were made using a one-step procedure, with APTES fulfilling the role as the base catalyst as well as providing surface amines for cross-linking sites. A two-step procedure using acid hydrolysis, followed by APTES-catalyzed condensation, was followed for TEOS-derived aerogels. The TMOS-derived monoliths had a bulk density of 0.28 g/cm^3 versus 0.25 g/cm^3 for TEOS-derived aerogels. This is most likely due to slightly less shrinkage of the TEOS aerogels upon supercritical drying (20.6% vs 26.5%). Thermal conductivity measured on 4.7 cm disks of 3.2 mm thickness using a modified guarded hot-plate technique ranged from 20 mW/m · K for TEOS-derived aerogels to 22 mW/m · K for TMOS-derived aerogels, possibly reflecting their slight density differences. The TEOS-derived aerogels also had a slightly lower modulus from compression (15.5 MPa vs 22.2 MPa for TMOS-derived aerogels). As evidenced by solid ^{13}C NMR spectra of cross-linked monoliths derived from TEOS and TMOS, the amount of cross-linking was virtually indistinguishable between the TEOS- and TMOS-derived samples. Integration of the methyl group from the isopropylidene moiety from BPGE (42 ppm) with the APTES peak (9 ppm) suggests an average of about 1.5 epoxy units for every two amines for this formulation. Solid ^{29}Si NMR for both TEOS- and TMOS-derived aerogels also showed virtually no difference. Both spectra contained a broad peak at −65 ppm for the APTES-derived T_3 silicon and

two broad peaks at −99 and −108 ppm for the TEOS- or TMOS-derived Q_3 and Q_4 silicons, respectively.

Optimization Study. After it was verified that the molecular structure and properties are virtually identical between the TEOS- and TMOS-derived aerogels and BPGE was identified as the preferred epoxy cross-linker, a study was conducted to optimize the properties of the TEOS-derived aerogels made from ethanol. Several preparation conditions were varied in the optimization study, including the concentration of the total Si in the initial sol (0.8−1.6 mol/L), the fraction of the total Si derived from APTES (15−45 mol %), and the amount of BPGE in the monomer bath (15−25 w/w % of the total solution). Ranges of the total Si concentration and the APTES fraction were based on the results from the initial screening study, where aerogels made from higher than 45 mol % APTES in combination with lower than 0.8 mol/L total Si were extremely difficult to handle, especially before cross-linking.

In addition, as noted, we have observed more shrinkage and more solvent remaining in the ethanol-derived aerogels after supercritical fluid extraction. Both of these issues may simply be due to less solubility of ethanol in liquid CO_2 than other solvents previously used in the polymer-cross-linked systems. With diisocyanate cross-linked aerogels, we have observed a reduction in shrinkage as well as an improvement in the elastic properties by substituting a portion of the TMOS-derived silicon with BTMSH (14). Hence, we examine the effect of incorporating BTMSH into the aerogels derived from TEOS and cross-linked with epoxy in an ethanol solution. Thus, a fourth variable studied was the amount of Si derived from BTMSH, which was adjusted from 0 to 40 mol %, noting that each BTMSH molecule provides two atoms of Si. A d-optimal design strategy was utilized to minimize the number of experiments necessary to evaluate a full quadratic model in all four variables. A total of 26 different batches of aerogels were prepared in all, including five repeats of one formulation to assess model reliability and accuracy. Preparation conditions and measured results are listed in Table 2 in the random run order followed experimentally.

Solid ^{29}Si NMR spectra of four representative runs from Table 2 are shown in Figure 2. APTES- and BTMSH-derived Si peaks overlap completely in the finished aerogels. Figure 2a shows a spectrum of an aerogel monolith from run 1 made using 15 mol % APTES and no BTMSH. The APTES-derived Si (T_3 peak) is assigned to the broad peak at −65 ppm. The spectrum in Figure 2b in comparison is from a monolith made from 45 mol % APTES and no BTMSH (run 7) and differs from Figure 2a in the relative size of the APTES T_3 peak (−65 ppm) compared to TEOS-derived Si (Q_3 peak at −100 ppm and Q_4 peak at −110 ppm). The spectra from aerogels made using 40 mol % BTMSH are shown in parts c (run 4 with 15 mol % APTES) and d (run 8 using 45 mol % APTES) of Figure 2. Figure 2d is nearly identical with Figure 2b except that the TEOS peaks (which account for only 15 mol % of total Si in this run) at −100 and −110 ppm are very small. The one large peak in the spectrum at −65 ppm

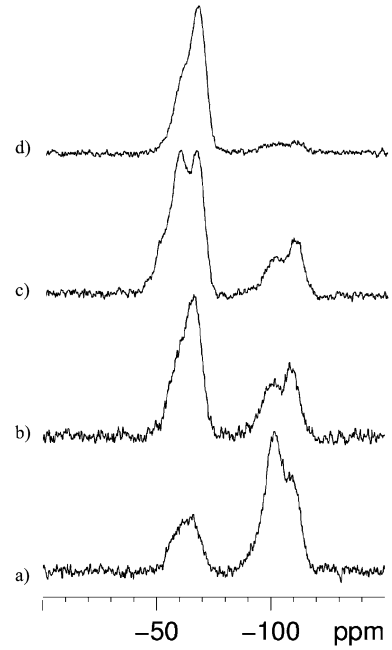

FIGURE 2. Solid ^{29}Si NMR of monoliths from runs listed in Table 2, including (a) run 1 made from 15 mol % APTES Si and no BTMSH, (b) run 7 made from 45 mol % APTES Si and no BTMSH, (c) run 4 made from 15 mol % APTES Si and 40 mol % BTMSH Si, and (d) run 8 made from 45 mol % APTES Si and 40 mol % BTMSH Si.

is from the T_3 peak, which accounts for Si derived from both BTMSH and APTES, showing that condensation goes to completion for these monomers. The spectrum shown in Figure 2c has an extra peak at −55 ppm, which must be due to less than fully reacted BTMSH-derived Si (T_2 peak). With APTES at only 15 mol % in this monolith, it might not have been basic enough in the initial sol to fully condense all of BTMSH. Similar results were seen in other aerogels in the study made with this combination of low APTES and high BTMSH. The addition of a small amount of ammonium hydroxide or other base catalyst should drive condensation to completion.

Empirical models of measured properties shown in Table 2 were derived using multiple linear least-squares regression as previously described. Response surfaces for dimensional shrinkage over the entire process of making the monoliths versus the total Si concentration and APTES mol % are shown in parts a (no BTMSH) and b (40 mol % BTMSH-derived Si) of Figure 3. All variables are significant predictors of shrinkage with standard error = 0.11% and $R^2 = 0.95$. The most striking observation is that pronounced shrinkage is observed when no BTMSH is used, especially when the epoxy concentration, total Si, and APTES concentration are low. As the APTES and total Si concentrations increase, the number of amine sites available for cross-linking increases, and hence the amount of cross-linking increases. Thus, the amount of reinforcement through cross-linking has a direct effect on the ability of the porous structure to resist shrinkage. In contrast, when 40 mol % BTMSH is used, less shrinkage is observed overall with very little added effect from the total Si, APTES, or epoxy concentration. This may be due to the fact that the more compliant hexane linkages in the silica backbone allow the aerogel to spring back after

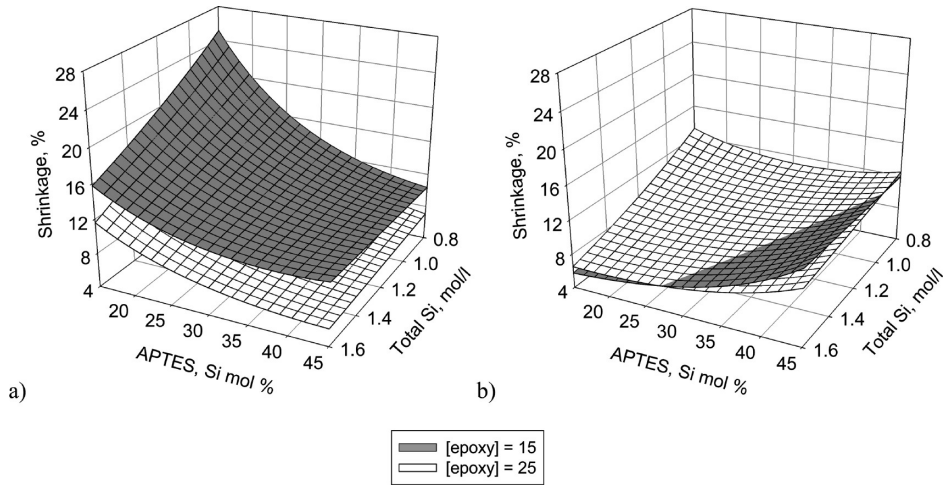

FIGURE 3. Graphs of the empirical model for shrinkage plotted versus the fraction of Si derived from the APTES and total Si concentration with (a) no BTMSH-derived Si and (b) 40 mol % BTMSH-derived Si.

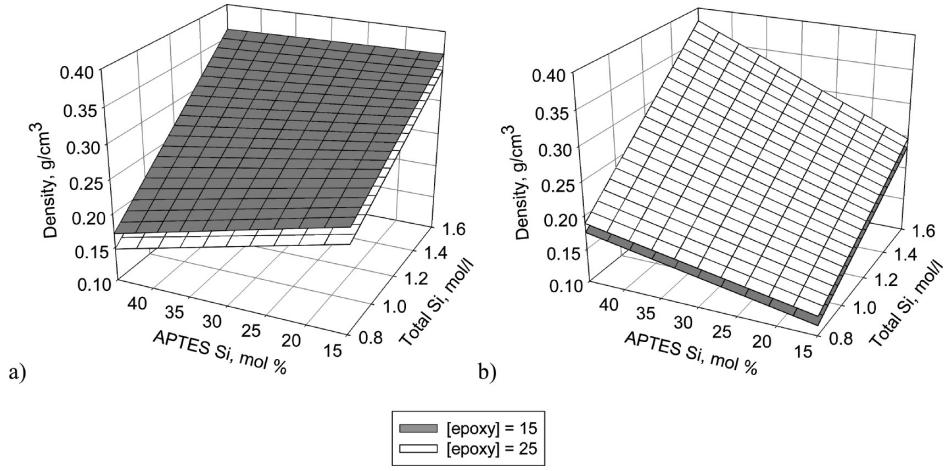

FIGURE 4. Graphs of the empirical model for density plotted versus the fraction of Si derived from the APTES and total Si concentration with (a) no BTMSH-derived Si and (b) 40 mol % BTMSH-derived Si.

drying or to resist shrinkage similar to the way polymer cross-linking does.

The density ranged from 0.1 g/cm^3 to nearly 0.4 g/cm^3 across the whole study. Graphs of the empirical model for the density versus the total Si concentration and the APTES fraction are shown in parts a (no BTMSH) and b (40 mol % BTMSH-derived Si) of Figure 4. All variables are significant predictors of the density with standard error = 0.015 g/cm^3 and R^2 = 0.98. As expected, the most influential variable on the density is the total Si concentration. Increasing the total Si increases the density of the underlying silica backbone and also increases the number of amine sites available for cross-linking even at the same level of the APTES fraction. In the absence of BTMSH, decreasing the epoxy concentration and the APTES fraction causes the density to increase because of the greater shrinkage as observed in Figure 3a. When 40 mol % BTMSH is used, shrinkage is less of a factor. Thus, increasing the APTES fraction and increasing the epoxy concentration have the expected effect of increasing the density through an increase in the amount of polymer cross-linking.

Similar but opposite trends are seen for the percent porosity calculated from the measured bulk density (ρ_b) and the skeletal density (ρ_s) measured by helium pycnometry using eq 1.

Graphs of the model for porosity are shown in Figure 5. Again, all four variables are statistically significant, with

$$\text{porosity } \% = (1/\rho_b - 1/\rho_s)/(1/\rho_b) \times 100 \qquad (1)$$

standard error = 1.51 % and R^2 = 0.96. Overall, increasing the total Si concentration decreases the porosity as expected. In monoliths made using no BTMSH (Figure 5a), increasing the epoxy concentration slightly increases the porosity, which is attributed to greater shrinkage in the lower epoxy runs. At low Si concentration, increasing the APTES fraction causes a decrease in the porosity, while at higher total Si concentration, there is very little change in the porosity due to the APTES fraction. This observation is again most likely due to the greater dependence of the APTES fraction on shrinkage when no BTMSH is used. With monoliths made from 40 mol % BTMSH-derived Si (Figure 5b), increasing both the APTES fraction and epoxy concentration decreases the porosity slightly as expected because of a greater amount of polymer cross-linking.

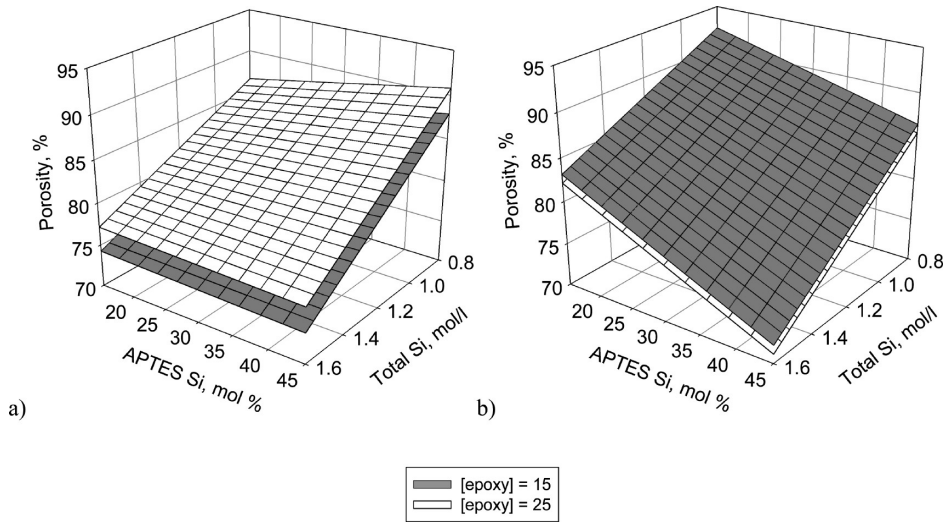

FIGURE 5. Graphs of the empirical model for porosity plotted versus the fraction of Si derived from the APTES and total Si concentration with (a) no BTMSH-derived Si and (b) 40 mol % BTMSH-derived Si.

Scanning electron micrographs (SEMs) of representative monoliths from Table 2 are shown in Figure 6a–h. Parts a–d of Figure 6 are all of monoliths made using 15 mol % APTES. A monolith from run 1 shown in Figure 6a made using 1.6 mol/L of total Si and no BTMSH has a very uniform distribution of particles and pores. In contrast, Figure 6b shows a monolith from run 4 made under the same conditions except that 40 mol % BTMSH-derived Si was used. This micrograph clearly shows that the porosity of the sample from run 4 is much more open while the density is about a third less than that for run 1, illustrating the shrinkage differences between samples with and without BTMSH added. Monoliths in parts c (run 14, no BTMSH) and d (run 16, 40 mol % BTMSH-derived Si) of Figure 6 are both made using 0.8 mol/L total Si and show a similar trend with a more uniform distribution of pore sizes and a higher density in the sample made with no BTMSH versus a wider distribution of pore sizes and a lower density for the sample made using 40 mol % BTMSH-derived Si.

Parts e–h of Figure 6 are graphs of monoliths made using 45 mol % APTES. A monolith from run 22 shown in Figure 6e made using 1.6 mol/L total Si and no BTMSH again has a more uniform distribution of particles and pores in contrast to Figure 6f, which shows a monolith from run 23 made under the same conditions except that 40 mol % BTMSH-derived Si was used. Here, the particles appear larger and clustered together compared to the sample with no BTMSH (Figure 6e). However, unlike monoliths made using 15 mol % APTES (Figure 6a,b), the density does not change as much between the monoliths made with (Figure 6f) and without BTMSH (Figure 6e). Monoliths shown in parts g (run 17, no BTMSH) and h (run 19, 40 mol % BTMSH) of Figure 6 are both made using 0.8 mol/L total Si. These again show a similar trend with a more uniform distribution of pores in the sample made with no BTMSH, though the pore sizes are larger than those in the corresponding samples made using 15 mol % APTES shown in Figures 6c and d. Although a wider distribution of pore sizes and larger clustered particles

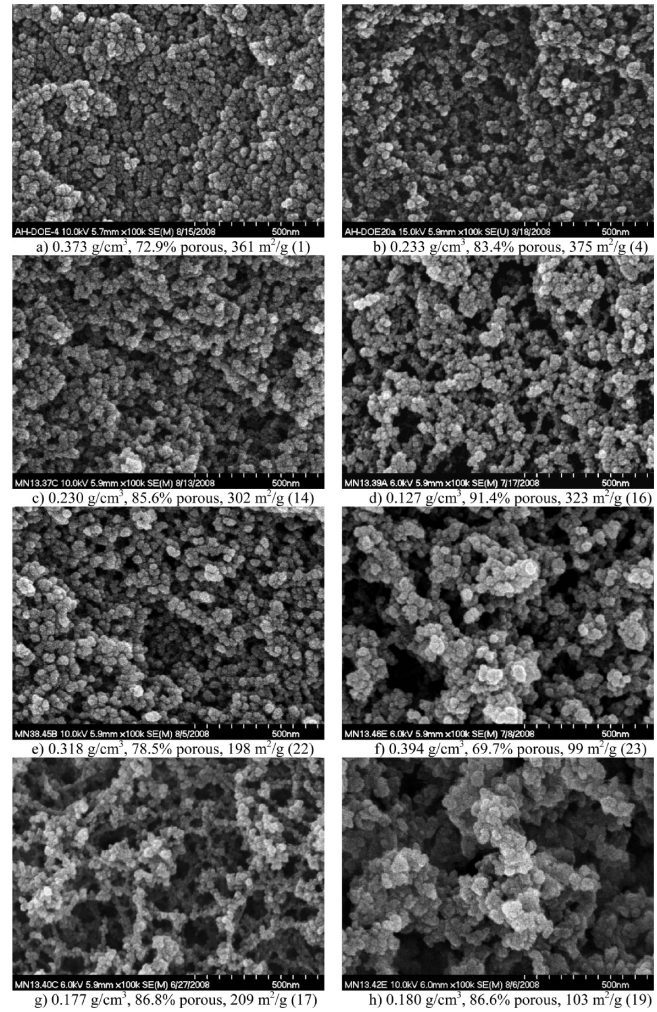

FIGURE 6. Side-by-side comparisons of micrographs of samples from Table 2 with (left) no BTMSH and (right) 40 mol % BTMSH-derived Si, including samples prepared with 1.6 mol/l total Si (15 mol % APTES) (a and b), with 0.8 mol/L total Si (15 mol % APTES) (c and d), with 1.6 mol/L total Si (45 mol % APTES) (e and f), and with 0.8 mol/L total Si (45 mol % APTES) (g and h). Sample numbers are shown in parentheses.

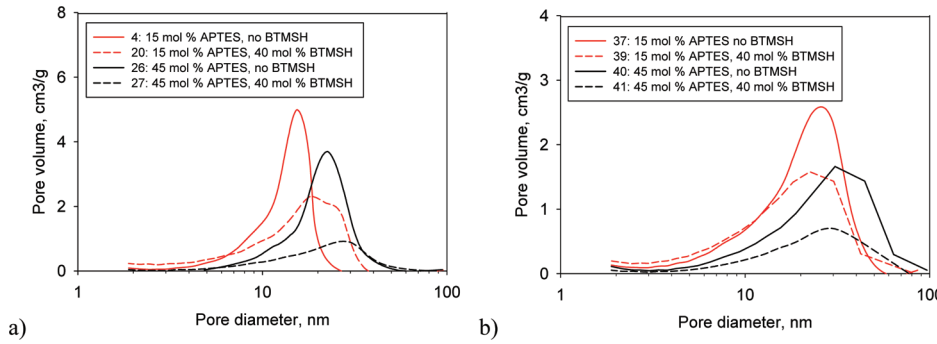

FIGURE 7. Desorption plots shown for selected samples from Table 2 at (a) 1.6 mol/L total Si and (b) 0.8 mol/L total Si.

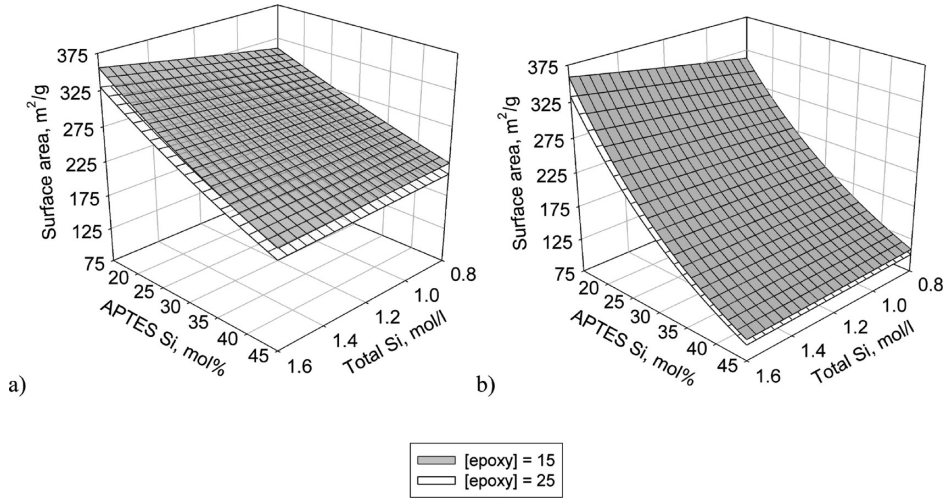

FIGURE 8. Graphs of the empirical model for surface area plotted versus the fraction of Si derived from the APTES and total Si concentration with (a) no BTMSH-derived Si and (b) 40 mol % BTMSH-derived Si.

for the sample made using 40 mol % BTMSH-derived Si are observed, the densities of samples shown in Figures 6g and h are virtually the same.

Mean pore diameter and surface area measurements were derived from nitrogen sorption data for all of the samples using the Brunauer–Emmett–Teller (BET) method and are listed in Table 2. Surface areas are also listed under the micrographs in Figure 6. The pore size measured by nitrogen sorption is known to be underestimated for aerogels because of contraction of the structure (15). Nevertheless, observed trends are consistent with that seen by SEM. Graphs of pore volume versus pore diameter are shown in Figure 7. Figure 7a shows a comparison of samples made using 1.6 mol/L total Si with low and high APTES and BTMSH. Note that the sharpest pore-size distribution is for the monolith made with 15 mol % APTES and no BTMSH. Increasing both APTES and BTMSH leads to larger pore diameters and wider pore distributions as seen by SEM. This is consistent with the observation that the pore size in silsesquioxane-derived aerogels roughly increases with the size of the organic bridge (7, 16). In Figure 7b, where the aerogel monoliths are made using 0.8 mol/L total Si, a larger distribution of pore sizes with increasing APTES and BTMSH is also seen. However, the measured pore diameter does not increase as much in response to increasing BTMSH.

As illustrated in the micrographs shown in Figure 6a–h, surface areas are much less sensitve to changes in the total Si and fraction of BTMSH-derived Si when 15 mol % APTES is used (surface areas ranged from 300 to 375 m^2/g). When 45 mol % APTES is used, however, surface areas are about halved when going from 0 to 40 mol % BTMSH-derived Si, possibly because of the increased particle size and clustering of particles observed by SEM (Figure 6e–h), when both APTES and BTMSH are in high concentration. Surface area models (standard error = 0.05; $R^2 = 0.99$) graphed in parts a (no BTMSH) and b (40 mol % BTMSH derived Si) of Figure 8 further reinforce these observed trends. The total Si concentration has only a small though significant effect on the surface area. Likewise, increasing the epoxy concentration accounts for only a small drop in the surface area. The fraction of Si derived from APTES has the largest effect on the surface area. As APTES mol % is increased, the surface area decreases, especially when BTMSH is at a high where the surface area drops from 370 m^2/g for 15 mol % APTES to 100 m^2/g for 45 mol % APTES. When no BTMSH is used, particle sizes are smaller and more uniformly distributed and surface areas drop by only 150 m^2/g over the entire range of the APTES fraction.

Mechanical Characterization. Compression tests were also performed on all runs listed in Table 2. Typical stress–strain curves for two different runs from Table 2 are shown in Figure 9a. Young's modulus taken from the initial slope of the stress–strain curves was modeled using multiple

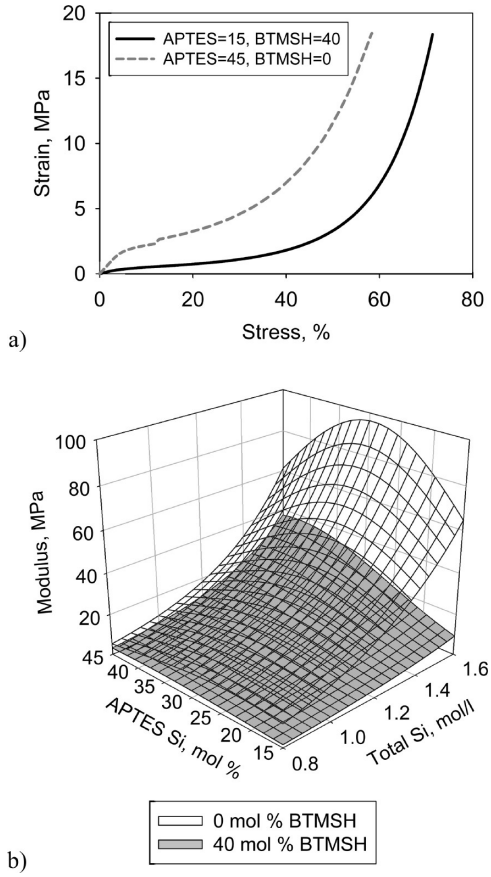

FIGURE 9. Typical stress−strain curves from compression testing of aerogel monoliths (a), shown with an empirical model of the modulus from compression graphed versus the total Si concentration and fraction of APTES-derived Si (b).

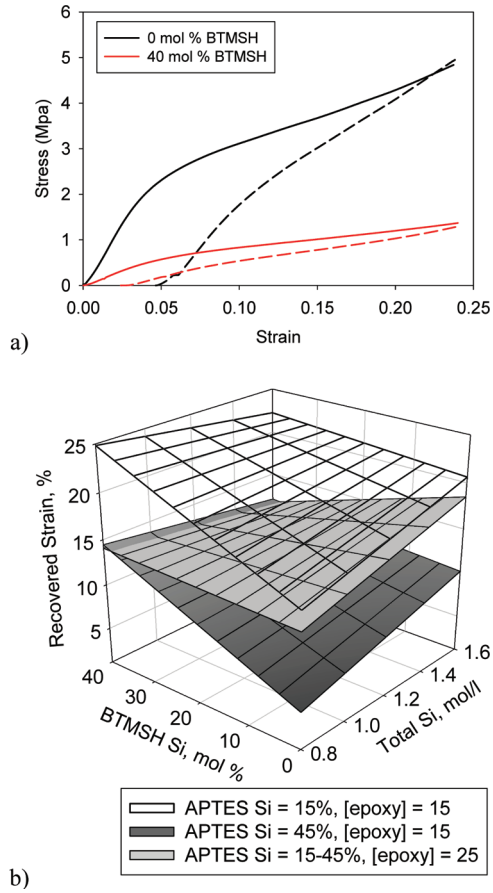

FIGURE 10. (a) Stress−strain curves for repeat compression tests of monoliths from Table 2 taken to 25% strain, where the solid lines are the first compression and the dotted lines are the second compression, and (b) graphs of empirical models for recovered strain after compression to 25% strain graphed versus the total Si concentration and fraction of BTMSH-derived Si.

linear regression analysis. Graphs of the empirical model for the modulus (standard error = 0.31; $R^2 = 0.94$) are shown in Figure 9b, where it is seen that the total Si concentration and APTES and BTMSH Si mole fractions are all significant predictors of the modulus. Including BTMSH-derived Si in the underlying silica is shown to decrease the modulus. The hexane linkages being more flexible effectively softens the silica backbone structure. Increasing the APTES-derived Si increases the modulus by increasing the sites available for polymer cross-linking. However, after a certain concentration of APTES, the surface may become saturated with amine sites and more APTES may end up inside the secondary particle structures and be unavailable for cross-linking. At this point, being that APTES has fewer alkoxy sites that can cocondense, it may also decrease the modulus by making the silica structure more flexible, similar to the way in which using methyltrimethoxysilane has been shown to increase the flexibility of aerogels (17). In monoliths where no BTMSH is used, the modulus is predicted to reach a maximum at 25−30 mol % APTES-derived Si for all levels of total Si. Beyond this level of APTES, the surfaces must be saturated with amine and no further amount will increase cross-linking. The highest modulus across the design is predicted to be 95 MPa for monoliths made using 1.6 mol/L total Si with 30 mol % APTES and no BTMSH. Such a monolith is predicted to have a density of 0.35 g/cm^3, a porosity of 76%, and a surface area of 270 m^2/g.

In contrast, using 40 mol % Si from BTMSH, the modulus is predicted to reach a maximum of 37 MPa at the highest APTES loading studied and 1.6 mol/L total Si. Two formulations under these conditions were made as a part of the experimental design study. Run 8 in Table 2 prepared using 15 w/w % epoxy had a measured modulus of 30 MPa, while run 23 in Table 2 prepared with 25 w/w % epoxy had a measured modulus of 49 MPa. Because more epoxy increases the modulus in this case, it would imply that more APTES amines are available on the surface for cross-linking. This is surprising in light of the fact that the finished surface areas of these monoliths are much reduced (∼100 m^2/g). However, BTMSH may increase the available surface area in the gel state by opening up the silica structure somewhat, as shown in Scheme 2. The clustering of the particles observed by SEM (and concomitant reduction in the surface areas) may be happening during cross-linking (and may even be due to an increased level of cross-linking) or after cross-linking during the drying process.

Over the whole study, the epoxy concentration was not found to have a significant effect on the modulus over and above random error in the study. However, this may be due to the differential shrinkage masking the effect of the epoxy concentration on the modulus. Increasing shrinkage in-

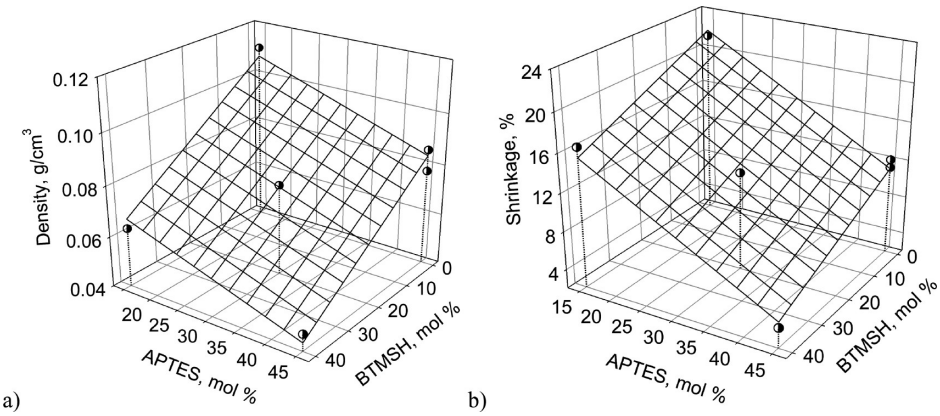

FIGURE 11. Empirical models for (a) density and (b) shrinkage from runs in Table 3 graphed versus the fraction of APTES- and BTMSH-derived Si.

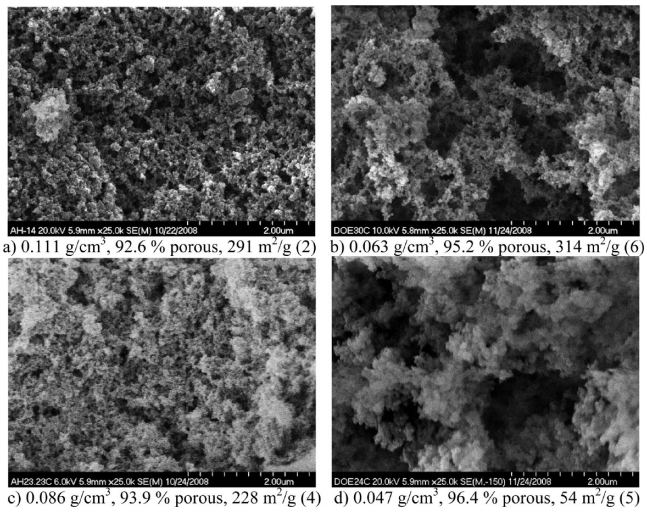

FIGURE 12. Side-by-side comparisons of micrographs of samples from Table 3 with (left) no BTMSH and (right) 40 mol % BTMSH-derived Si, including samples prepared using (a and b) 15 mol % APTES-derived Si and (c and d) 45 mol % APTES-derived Si. Sample numbers are in parentheses.

creases the density and increasing density increases the modulus, but increasing the epoxy concentration decreases shrinkage when no BTMSH is used and has no effect on shrinkage at high BTMSH concentration.

To assess the elastic recovery of the aerogel monoliths, repeat compression tests were run where the samples were compressed to 25% strain twice and allowed to recover. Typical stress–strain curves for repeat compression tests are shown in Figure 10a for monoliths made using 1.6 mol/L total Si and 15 mol % APTES from run 1 (no BTMSH) and run 4 (40 mol % BTMSH). As shown, samples with high amounts of BTMSH tended to more closely retrace the first stress–strain curve on the second compression and recover more than samples with no BTMSH. This is again due to obtaining a more compliant silica backbone by including the hexyl linkages. A graph of the empirical model (standard deviation = 3.1 %; $R^2 = 0.7$) for recovered strain after the first compression versus the BTMSH fraction and total Si is shown in Figure 10b. This graph shows that, for monoliths made from 15 mol % APTES, 15 w/w % epoxy, and 40 mol % BTMSH, recovery is nearly complete after compression to 25% strain, especially for monoliths made with the lowest total Si concentration. Higher APTES loadings or epoxy concentrations tend to reduce elastic recovery for all levels of total Si and BTMSH fraction. This suggests that the increase in cross-linking due to both higher APTES and higher epoxy concentration restricts the secondary particles from flexing, leading to a more permanent deformation of the aerogel monoliths on compression.

Lower-Density Monoliths. Because decreasing the total Si concentration is also predicted to increase elastic recovery after compression, six additional monoliths were made using a total Si concentration of 0.4 mol/L to see if recovery could be further improved at even lower density. These results, with APTES and BTMSH fractions varied as before and the epoxy concentration held constant at 15 w/w %, are summarized in Table 3. In these runs, densities ranged from 0.047 to 0.111 g/cm^3 and, as seen with higher total Si runs, were highly influenced by dimensional shrinkage during processing. Graphs of empirical models for shrinkage (standard error = 1.1 %; $R^2 = 0.98$) and density (standard error = 0.005 g/cm^3; $R^2 = 0.97$) along with the raw data are shown in Figure 11. Both shrinkage and density are shown to significantly decrease with increasing BTMSH and APTES concentrations, although the density should be expected to increase with an increased number of amine sites because of higher amounts of cross-linking. Thus, as seen with higher total Si runs, the aerogel density is highly influenced by dimensional shrinkage during processing.

Micrographs of monoliths from Table 3 made from 0.4 mol/L total Si are shown in Figure 12a–d, noting that the magnification is not as high as that shown in Figure 6. However, they exhibit trends similar to those of higher total Si containing monoliths, where particle clustering and the distribution of pore sizes increase as the amounts of APTES and BTMSH are increased. Figure 12a shows a monolith made using 15 mol % APTES and no BTMSH (run 2 from Table 3) with a fairly even distribution of pores, most of which appear to be smaller than 20 nm. In comparison, the sample made under the same conditions with 40 mol % BTMSH (run 6 in Table 3) shown in Figure 12b also has some much larger pores, on the order of 2 μm. Similarly, when samples made from 45% APTES are compared, the same

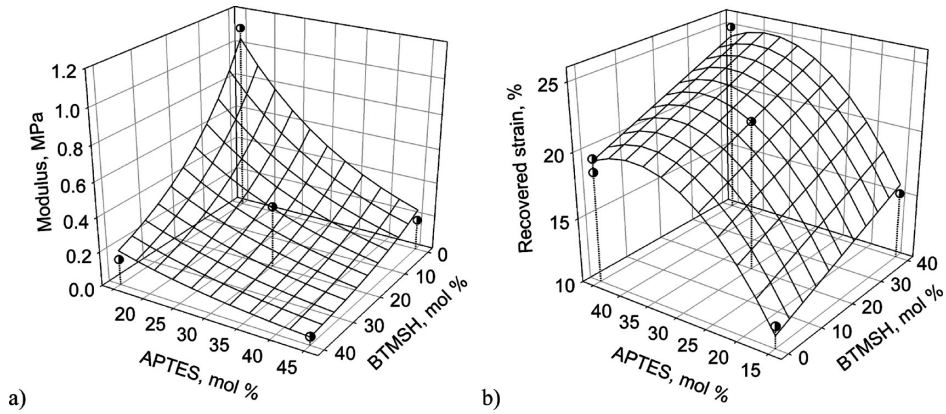

FIGURE 13. Empirical models and raw data for (a) modulus and (b) recovered strain graphed versus the fraction of APTES and BTMSH-derived Si for monoliths from Table 3.

large increase in the pore size is observed going from monoliths made with no BTMSH (Figure 12c, run 4 from Table 3) and with 40 % BTMSH (Figure 12d, run 5 from Table 3). Surface areas measured by BET follow trends seen in the higher-density aerogels listed in Table 2. Surface areas listed in Figure 12 do not change when going from 0 to 40 mol % Si from BTMSH when 15 mol % APTES Si is used. However, they do decrease dramatically when 45 mol % APTES is used, dropping from 228 m^2/g when no BTMSH is used down to 54 m^2/g for monoliths made with 40 mol % Si from BTMSH.

Response surface models for Young's modulus and elastic recovery after compression to 25 % strain for runs using 0.4 mol/L total Si concentration are graphed versus the APTES and BTMSH Si mole fractions and are shown in Figure 13. The empirical model for the modulus (standard error = 0.46; $R^2 = 0.92$) is shown in Figure 13a. The modulus significantly decreases with increasing BTMSH concentration, as seen with higher total Si concentration. However, in contrast to monoliths made using higher total Si, increasing the APTES concentration is seen to decrease the modulus when the total Si concentration is 0.4 mol/L, especially for monoliths prepared with no BTMSH. This may be due again to the influence of shrinkage and the fact that higher density usually leads to increases in the modulus.

The empirical model for recovered strain after compression to 25 % strain (standard error = 0.011 %; $R^2 = 0.98$) for runs from Table 3 using 0.4 mol/L total Si (Figure 13b) shows that elastic recovery increases with increasing BTMSH concentration in agreement with monoliths prepared from higher total Si concentration. However, different from higher Si runs, increasing the APTES concentration also increases the amount of recovered strain for 0.4 mol/L total Si. Indeed, complete recovery from 25 % strain is seen for run 5 from Table 3, made using 45 mol % APTES and 40 mol % BTMSH. This sample was also subjected to compression to 50 % strain, as seen in Figure 14. A 2.30 cm specimen is shown before compression (Figure 14a), at 50 % strain (Figure 14b), and after two cycles of compression (Figure 14c), having lost only 2.6 % of the initial length.

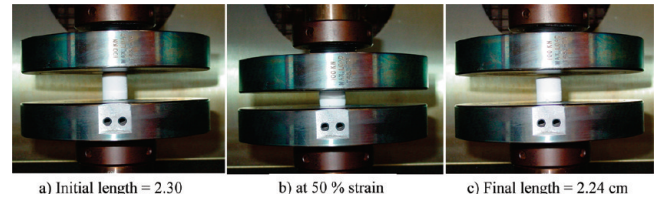

FIGURE 14. Repeat compression test of the sample from Table 3, run 5 taken to 50% strain.

CONCLUSIONS

It has been demonstrated that less toxic TEOS and ethanol can be used to synthesize silica aerogels cross-linked with ethanol-soluble epoxies, achieving increases in mechanical properties comparable to those previously studied in diisocyanate-cross-linked aerogels. The use of ethanol as the solvent, in particular, improves the viability of large-scale manufacturing of the polymer-cross-linked aerogels because large amounts of solvent (from the initial gelation through diffusion of the monomer into the alcogels and additional rinsing steps) are used in the production. Additionally, empirical models were generated for the prediction of the properties of the epoxy-cross-linked aerogels over a wide range of densities as well as for the identification and understanding of significant relationships between the processing parameters and final properties. In this way, the combination of properties (mechanical strength, surface area, density, etc.) can be tailored to a specific application. For example, if a high modulus is desired, it is predicted to be at a maximum of 95 MPa for aerogels made from 1.6 mol/L total Si (30 mol % derived from APTES). However, if more flexible aerogel monoliths are desired, vastly improved elastic recovery from compression up to as much as 50 % strain can be obtained using 0.4 mol/L total Si (45 mol % derived from APTES and 40 mol % from BTMSH). The use of BTMSH also greatly reduces dimensional shrinkage occurring over the fabrication process from the initial gelation to supercritical fluid extraction for cross-linked aerogels made in ethanol.

Acknowledgment. We gratefully acknowledge financial support from NASA's Fundamental Aeronautics Program, NASA's Innovative Partnerships Program, and the Undergraduate Student Researcher Program. We thank Dr. Baochau

N. Nguyen of the Ohio Aerospace Institute for running solid NMR and Anna Palczer for porosimetry measurements.

REFERENCES AND NOTES

(1) (a) Pierre, A. C.; Pajonk, G. M. *Chem. Rev.* **2002**, *102*, 4243–4265. (b) Morris, C. A.; Anderson, M. L.; Stroud, R. M.; Merzbacher, C. I.; Rolison, D. R. *Science* **1999**, *284*, 622–624. (c) Pajonk, G. M. *Catal. Today* **1999**, *52*, 3–13.

(2) (a) Zhang, G.; Dass, A.; Rawashdeh, A.-M. M.; Thomas, J.; Counsil, J. A.; Sotiriou-Leventis, C.; Fabrizio, E. F.; Ilhan, F.; Vassilaras, P.; Scheiman, D. A.; McCorkle, L.; Palczer, A.; Johnston, J. C.; Meador, M. A. B.; Leventis, N. *J. Non-Cryst. Solids* **2004**, *350*, 152–164. (b) Leventis, N.; Sotiriou-Leventis, C.; Zhang, G.; Rawashdeh, A.-M. M. *Nano Lett.* **2002**, *2*, 957–960.

(3) Meador, M. A. B.; Capadona, L. A.; McCorkle, L.; Papadopoulos, D. S.; Leventis, N. *Chem. Mater.* **2007**, *19*, 2247–2260.

(4) Katti, A.; Shimpi, N.; Roy, S.; Lu, H.; Fabrizio, E. F.; Dass, A.; Capadona, L. A.; Leventis, N. *Chem. Mater.* **2006**, *18*, 285–296.

(5) Meador, M. A. B.; Fabrizio, E. F.; Ilhan, F.; Dass, A.; Zhang, G.; Vassilaras, P.; Johnston, J. C.; Leventis, N. *Chem. Mater.* **2005**, *17*, 1085–1098.

(6) (a) Ilhan, U. F.; Fabrizio, E. F.; McCorkle, L.; Scheiman, D. A.; Dass, A.; Palczer, A.; Meador, M. A. B.; Johnston, J. C.; Leventis, N. *J. Mater. Chem.* **2006**, *16*, 3046–3054. (b) Mulik, S.; Sotiriou-Leventis, C.; Churu, G.; Lu, H.; Leventis, N. *Chem. Mater.,* **2008**, *20* (15), 5035–5046.

(7) (a) Ilharco, L. M.; Fidalgo, A.; Farinha, J. P. S.; Martinho, J. M. G.; Rosa, M. E. *J. Mater. Chem.* **2007**, *17*, 2195–2198. (b) Fidalgo, A.; Farinha, J. P. S.; Martinho, J. M. G.; Rosa, M. E.; Ilharco, L. M. *Chem. Mater.* **2007**, *19*, 2603–2609.

(8) Novak, B. M.; Auerbach, D.; Verrier, C. *Chem. Mater.* **1994**, *6*, 282–286.

(9) Wei, T. Y.; Lu, S. Y.; Chang, Y. C. *J. Phys. Chem. B* **2008**, *112*, 11881–11886.

(10) Shea, K. J.; Loy, D. A. *Chem. Mater.* **2001**, *13*, 3306–3319.

(11) Loy, D. A.; Carpenter, J. P.; Myers, S. A.; Small, J. H.; Greaves, J.; Shea, K. J. *J. Am Chem. Soc.* **1996**, *118*, 8501–8502.

(12) Oviatt, H. W., Jr.; Shea, K. J.; Small, J. H. *Chem. Mater.* **1993**, *5*, 943–950.

(13) (a) Nguyen, B. N.; Meador, M. A. B.; Tousley, M. E.; Shonkwiler, B. *Polym. Prepr. (Am. Chem. Soc., Div. Polym. Chem.)* **2008**, *49* (1), 340. (b) Nguyen, B. N.; Meador, M. A. B.; Tousley, M. E.; Shonkwiler, B.; McCorkle, L.; Scheiman, D. A.; Palczer, A. *ACS Appl. Mater. Interfaces* **2009**, *1*, 621–630.

(14) Vivod, S. L.; Meador, M. A. B.; Nguyen, B. N.; Quade, D. J.; Randall, J. P. *Polym. Prepr. (Am. Chem. Soc., Div. Polym. Chem.)* **2008**, *49* (2), 521.

(15) Scherer, G. W.; Smith, D. M.; Stein, D. *J. Non-Cryst. Solids* **1995**, *186*, 309–315.

(16) Loy, D. A.; Jamison, G. M.; Baugher, B. M.; Russick, E. M.; Assink, R. A.; Prabaker, S.; Shea, K. J. *J. Non-Cryst. Solids* **1995**, *186*, 44.

(17) (a) Rao, A. V.; Bhagat, S. D.; Hirashima, H.; Pajonk, G. M. *J. Colloid Interface Sci.* **2006**, *300*, 279–285. (b) Kanamori, K.; Aizawa, M.; Nakanishi, K.; Hanada, T. *Adv. Mater.* **2007**, *19*, 1589–1593.

AM900014Z